REPORT DOCUMENTATION PAGE

AFRL-SR-AR-TR-05-

0392

1. AGENCY USE ONLY *(Leave blank)*	2. REPORT DATE	3. REPORT TYPE AND DATES COVERED
		01 Jan 2002 - 31 Dec 2004 FINAL

4. TITLE AND SUBTITLE
HIGH FREQUENCY POLYMER BASED LOW LOSS INTEGRATED SYSTEMS

5. FUNDING NUMBERS
61102F
2301/AX

6. AUTHOR(S)
PROFESSOR FETTERMAN

7. PERFORMING ORGANIZATION NAME(S) AND ADDRESS(ES)
THE REGENT OF THE UNIV OF CALIFORNIA
1400 UEBERROTH BLDG BOX 951406
LOS ANGELES CA 90095

8. PERFORMING ORGANIZATION REPORT NUMBER

9. SPONSORING/MONITORING AGENCY NAME(S) AND ADDRESS(ES)
AFOSR/NE
4015 WILSON BLVD
SUITE 713
ARLINGTON VA 22203

10. SPONSORING/MONITORING AGENCY REPORT NUMBER
F49620-02-1-0029

11. SUPPLEMENTARY NOTES

12a. DISTRIBUTION AVAILABILITY STATEMENT
DISTRIBUTION STATEMENT A: Unlimited

12b. DISTRIBUTION CODE

13. ABSTRACT *(Maximum 200 words)*

We have demonstrated a polymer-based four-element photonic RF phase-shifter array in a single chip. By employing a novel design to remove the operational drawbacks of this type of device, four phase outputs were independently controlled with high linearity and negligible power fluctuation. A simple vertical stack of these devices can now be used to form an N x N photonic RF phase shifter array without increasing complexity that will contribute to the future photonic phased array systems.

In both fiber wireless and photonic time-stretching system, the power penalty due to the fiber chromatic dispersion effects is undesirable and limits the system perfonnance. We have demonstrated techniques to reduce this power penalty using both polymer-based SSS and DSB modulators. The limit on the modulation frequency due to this penalty can be almost completely eliminated with the SSB modulation without a bandwidth limItation and also can be significantly improved with the DSB modulation by using an alternative quadrature bias point. These results indicate that SSB mo4ulation or appropriately biased DSB modulation can have important roles in both CW and pulsed applications.

We report a PB induced optical modulator with dual-driving electrodes. The optical waveguides created support both TE and TM polarisations with low insertion loss, which could be thither reduced by optimising the PB time. The resulting device performances are comparable to that obtained in our earlier Work (9, lii developed using ~ a ridge-type optical waveguide, and are the first results operating at 1.55 pm wavelength in reported PB induced polymer modulators.

14. SUBJECT TERMS

15. NUMBER OF PAGES

16. PRICE CODE

17. SECURITY CLASSIFICATION OF REPORT	18. SECURITY CLASSIFICATION OF THIS PAGE	19. SECURITY CLASSIFICATION OF ABSTRACT	20. LIMITATION OF ABSTRACT
Unclassified	Unclassified	Unclassified	UL

Single-Chip Integrated Electro-Optic Polymer Photonic RF Phase Shifter Array

Jeehoon Han, *Senior Member, IEEE*, Byoung-Joon Seo, SeongKu Kim, Hua Zhang, and Harold R. Fetterman

***Abstract*—This paper demonstrates a four-element integrated photonic radio-frequency (RF) phase shifter array in a single chip with an advanced configuration. These devices are integrated using electrooptic polymer materials and involve several novel technologies. Measurements of this configuration showed that our four outputs were independent and had highly linear RF phases over 360° with negligible RF power fluctuation at the modulation frequency of 20 GHz. This significant improvement is capable of removing one of the major problems in using this type of phase shifter architecture.**

***Index Terms*—Beam-forming systems, optical single sideband (SSB) modulators, phased array antenna, photonic radio-frequency (RF) phase shifters.**

I. Introduction

PHASED array antennas using photonic radio-frequency (RF) phase shifters hold great promise for advanced wireless communications and radar applications due to their many advantages such as simple implementation, optical distribution capability, low cost, light weight, and small size [1]–[6]. They can control multiple RF phases using dc voltages and feed the independent phase outputs into an antenna array to perform rapid and continuous beam-forming functions. Among the possible phase shifter architectures, the one described in [1] is the simplest and most flexible approach. In actual implementation, one can integrate multiple phase shifters in a single chip providing multiple independent phase outputs. Such a phase shifter array can significantly reduce the complexity of RF distribution structures fed by a single RF and optical source. In contrast to microwave monolithic integrated circuit systems, the frequency bandwidth of these devices is very wide and effectively covers from dc to over 50 GHz. Also, it allows continuous beam-forming without limitation on the number of beam angles. This design of the phase shifter, however, suffers from a lack of phase shift linearity and a substantial amount of power variation as the phase is tuned.

Having recognized the requirements for practical usage, we present an advanced configuration for a four-element photonic RF phase shifter array. For these devices, our recently developed polymer materials and advanced fabrication technologies enabled flexible design and integration as well as broad bandwidth operation. Also, we discuss the new generation of phase-shifter architecture using a multimode interference (MMI) structure to further reduce the complexity.

Manuscript received March 18, 2003; revised July 29, 2003. This work was supported in part by AFOSR and DARPA.

J. Han, B.-J. Seo, S. Kim, and H. R. Fetterman are with the Electrical Engineering Department, University of California, Los Angeles, CA 90095 USA (e-mail: hoon@ee.ucla.edu).

H. Zhang was with Pacific Wave Industries, Los Angeles, CA 90024 USA. He is now with the Electrical Engineering Department, University of California, Los Angeles, CA 90095 USA.

Digital Object Identifier 10.1109/JLT.2003.819801

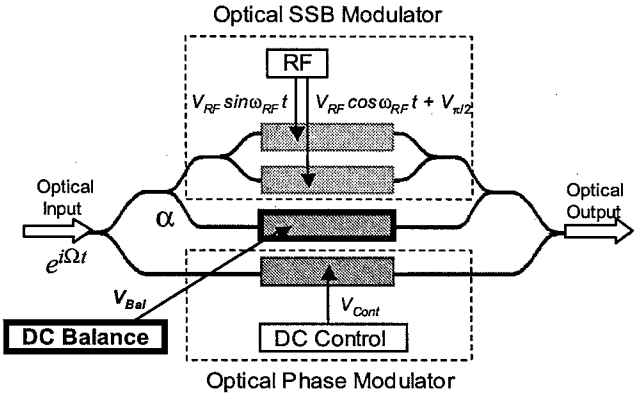

Fig. 1. Schematic diagram representing the balanced photonic RF phase shifter with a balancing arm. α represents the optical power-splitting ratio at the balancing arm.

II. Advanced Photonic RF Phase-Shifter Design

The architecture described in [1], which is analogous to the structure shown in Fig. 1 except for the balancing arm, consists of a single-sideband (SSB) modulator on one arm of a Mach–Zehnder (MZ) and an optical phase modulator on the other arm. The SSB modulator unit generates a carrier at Ω and a sideband at $\Omega + \omega_{\mathrm{RF}}$. On the other arm of the MZ, the control dc bias V_{Cont} is applied to the optical phase modulator to induce a phase-shifted optical carrier at Ω. Finally, the mixing of these signals in a photodiode gives rise to the RF signal at ω_{RF} with a variable phase controlled by V_{Cont}.

The calculated RF phase and power characteristics are shown in Figs. 2 and 3 as a function of control voltage at a modulation depth of 0.5. The phase of the RF signal can be controlled by changes in control voltage V_{Cont} and varies almost linearly up to 140°. However, it starts exhibiting a lack of linearity as the control voltage is tuned over $2V_{\pi}$. A maximum RF phase deviation of approximately 50° from the ideal linear characteristic is observed. In addition, the RF power exhibits fluctuation of approximately 15 dB as the control voltage is tuned over $2V_{\pi}$. For most practical applications, a wide range of linear phase shifting is required and the RF power fluctuation is very undesirable. Most of the detrimental effects are caused by the presence of the carrier signal from the SSB modulator unit [4]. This carrier signal is added to another phase shifted carrier signal at the same frequency Ω and mixed with the sideband in the photodiode. The resulting RF signal reveals degradation of phase

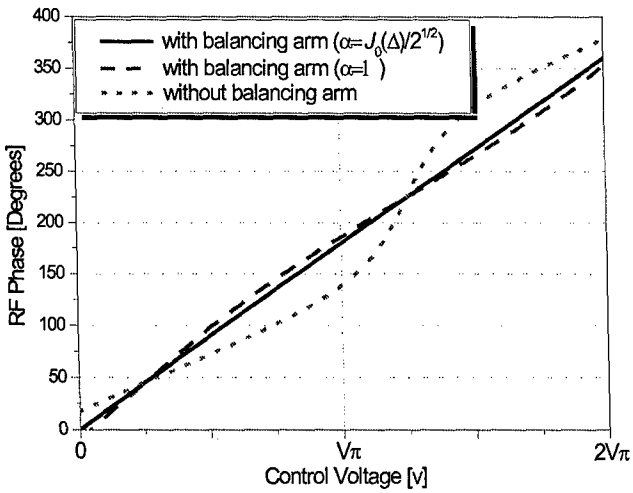

Fig. 2. The calculated RF phase characteristics as a function of control voltage at a modulation depth of 0.5.

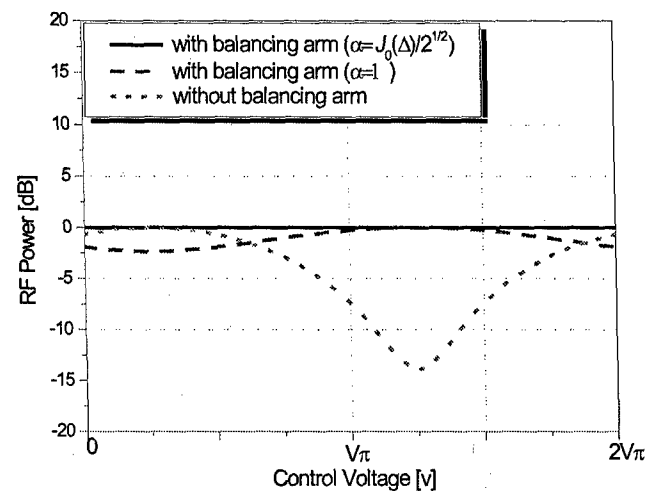

Fig. 3. The calculated RF power characteristics as a function of control voltage at a modulation depth of 0.5 (normalized to each maximum power).

and power characteristics. This effect is even more pronounced as the modulation depth is decreased. Choosing higher modulation depth tends to diminish these effects. This operating condition, however, is unfavorable in that it requires a considerable amount of RF source power and also generates harmonics and signal distortion. As a consequence, an alternative scheme with a reasonable modulation depth is required to extend the range of applications for these devices.

A simple solution has been developed to solve these problems under small signal operation. If the carrier signal is fully suppressed in the SSB modulator, these unwanted effects could be largely eliminated. Fig. 1 represents the schematic diagram for the balanced photonic RF phase shifter. This architecture inserts an additional arm in the inner MZ, which is intended to suppress the carrier signal in the SSB modulator so as to balance the system.

If the input optical signal with unit magnitude at a frequency of Ω is $E_{\text{in}}(t) = e^{i\Omega t}$, the output optical field and the resulting intensity at the modulation frequency ω_{RF} can be expressed as

$$E(t) = \frac{1}{4(1+\alpha)} e^{i\Omega t} \left[e^{i\Delta \sin(\omega_{\text{RF}} t)} + e^{i\Delta \cos(\omega_{\text{RF}} t) + i\frac{\pi}{2}} + 2\alpha e^{i\phi_{\text{Bal}}} + 2(1+\alpha) e^{i\phi_{\text{Cont}}} \right] \quad (1)$$

$$I_{\omega_{\text{RF}}}(t) = \frac{1}{4(1+\alpha)^2} A_{\text{RF}} J_1(\Delta) \cos(\omega_{\text{RF}} t + \varphi_{\text{RF}}) \quad (2)$$

where

$$A_{\text{RF}} = \Big\{ [J_0(\Delta) + 2\alpha \cos\phi_{\text{Bal}} + 2(1+\alpha)\cos\phi_{\text{Cont}}]^2 + [J_0(\Delta) + 2\alpha \sin\phi_{\text{Bal}} + 2(1+\alpha)\sin\phi_{\text{Cont}}]^2 \Big\}^{\frac{1}{2}} \quad (3a)$$

$$\varphi_{\text{RF}} = \tan^{-1}\left[\frac{J_0(\Delta) + 2\alpha \sin\phi_{\text{Bal}} + 2(1+\alpha)\sin\phi_{\text{Cont}}}{J_0(\Delta) + 2\alpha \cos\phi_{\text{Bal}} + 2(1+\alpha)\cos\phi_{\text{Cont}}} \right]. \quad (3b)$$

Here V_π is the half-wave voltage, $\Delta = \pi V_{\text{RF}}/V_\pi$ is the modulation depth, $\phi_{\text{Cont}} = \pi \cdot (V_{\text{Cont}}/V_\pi)$ is the optical phase shift by the control dc bias, $\phi_{\text{Bal}} = \pi \cdot (V_{\text{Bal}}/V_\pi)$ is the optical phase shift by the balancing dc bias, and α^2 is the optical power-splitting ratio at the balancing arm. The desired phase and magnitude of the optical signal in the balancing arm are established by the proper dc bias and splitting ratio, respectively.

The calculated RF phase and power characteristics of the balanced structure are shown in Figs. 2 and 3 in comparison with the structure without the balancing arm. For the choice of $\alpha = J_0(\Delta)/\sqrt{2}$ with $\phi_{\text{Bal}} = 5\pi/4$, the undesirable terms $J_0(\Delta)$ completely disappear (that is, the carrier signal is fully suppressed in the SSB modulator) and the ideal characteristics for the RF phase and power can be obtained such that

$$A_{\text{RF}}^2 = const., \quad \varphi_{\text{RF}} = \tan^{-1}\left[\frac{2\sin\phi_{\text{Cont}}}{2\cos\phi_{\text{Cont}}} \right] = \phi_{\text{Cont}}.$$

This indicates that the RF power does not vary at all and the RF phase shift is highly linear with respect to the control dc voltage, which makes these devices very suitable for optically controlled phase array antenna systems.

Assuming a simple symmetric splitting at the balancing arm, i.e., $\alpha = 1$, with $\phi_{\text{Bal}} = 5\pi/4$, this system shows a maximum phase deviation of less than 6° while maintaining the RF power fluctuation below 3 dB as the control voltage is tuned over $2V_\pi$. In this case, the carrier suppression in the SSB modulator is only partially accomplished since the balancing power is unequal to the carrier signal from the SSB modulator unit. Nevertheless, this significant improvement of nearly one order of magnitude is capable of removing one of the major problems in using this type of phase shifter architecture.

It is favorable to integrate multiple phase shifters in a single chip. This phase shifter array significantly reduces the complexity of RF feed structures and needs only a single RF and optical source. In a previous work, we have successfully demonstrated a compact two-element photonic RF phase shifter as a first step to development of an array of phase shifters [7]. This basic concept now has been extended to the advanced design in conjunction with the balanced architecture. The four-element phase-shifter array incorporating the balanced design is shown

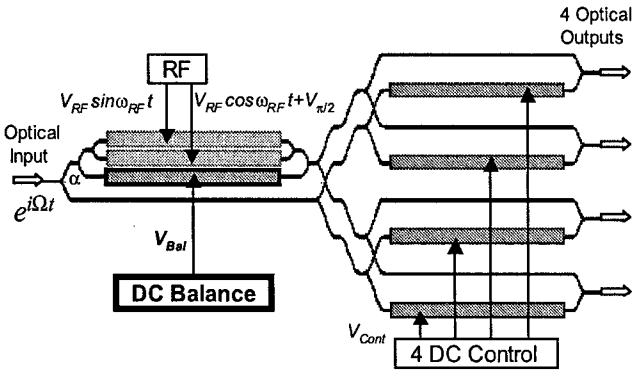

Fig. 4. The schematic diagram for the four-element RF phase shifter array with the balanced design.

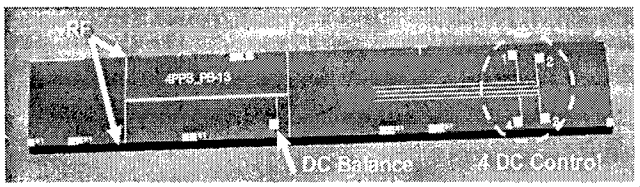

Fig. 5. The balanced multiple output photonic RF phase shifter fabricated in the APC-CPW polymer material.

in Fig. 4. The modulated optical output from the balanced SSB modulator is split into four branches and combined with the four outputs from the optical phase shifters. This signal distribution in a planar chip was achieved through the use of low crosstalk waveguide crossings and S-bend waveguide structures. The performance of these devices could be severely impacted by that of the optical waveguide crossings, and as such they were carefully implemented.

Fig. 5 shows the phase-shifter array in a single chip fabricated using recently developed polymer materials and advanced polymer fabrication technologies. The device size of the phase shifter with four outputs was 3.8 × 0.5 cm. For the simplicity of the design, the splitting ratio of the balancing arm α was set to be one. This guest-host system exhibits a high electrooptic coefficient, low material loss at 1.55 μm, and wide-band frequency response over 100 GHz [8]. The single-mode (SM) ridge optical waveguides were fabricated using the new inverted rib structures as shown in Fig. 6. The key benefit of these inverted rib structure is that it can eliminate damage problems of the core layer due to the photoresist solvents and etching processes [9]. This ultimately resulted in much simpler fabrication procedures and lower propagation losses. Also the SM waveguide structures were designed to provide the symmetric mode shape with a rib depth of 0.8 μm and waveguide width of 4 μm. A large optical nonlinearity in the core region was then achieved through the electrode poling. The microstrip lines with a characteristic impedance of 50 Ω were vertically aligned to the optical waveguides in the interaction regions, giving a traveling-wave configuration. For the minimum device length and insertion loss, raised-sine S-bend waveguide structures have been used in all the optical waveguide bending sections [10]. The test structures for the S-bend and waveguide crossings were fabricated on the same wafer. The measured bending losses of the S-bend structures were less than 0.2 dB. The measured excess optical loss due to the crossing was less than 0.5 dB, and the optical waveguide crossings exhibited a crosstalk level of less than −28 dB.

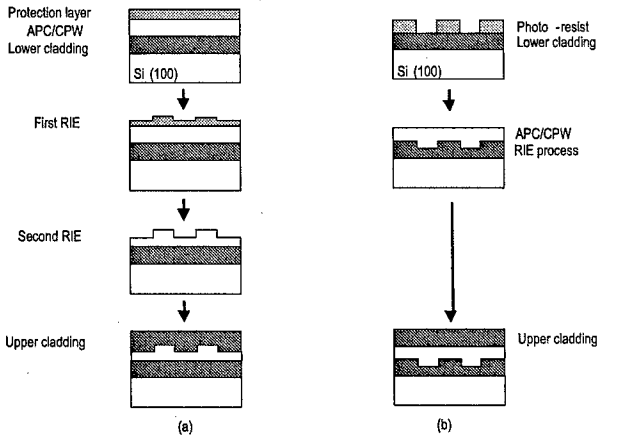

Fig. 6. Comparison of two fabrication procedures in (a) typical rib structures and (b) inverted rib structures.

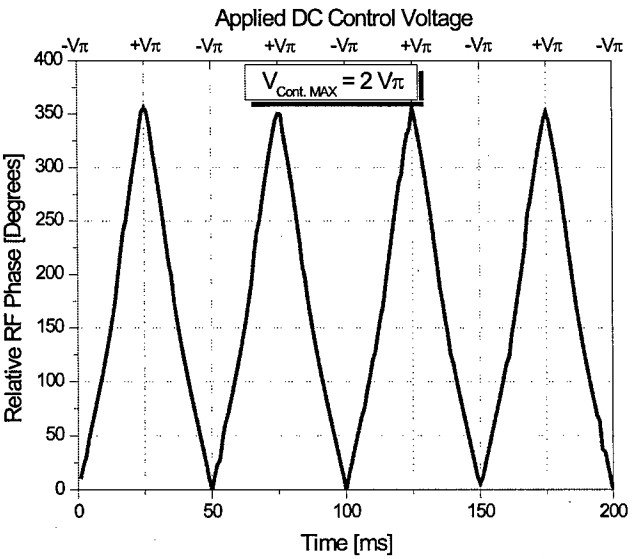

Fig. 7. The measured RF phase from a single output.

III. Measured Phase-Shifter Performance

The measured RF phase and power of a single element are shown in Figs. 7 and 8 at the modulation frequency of 20 GHz and modulation depth of 0.58. The performance of our phase shifter was measured using the experimental setup shown in Fig. 9. Triggering the HP 8510 network analyzer with the function generator allows the phase and power of the 20-GHz signal to be monitored as a function of time synchronized to the triangular control voltage. The linear relationship between voltage and time in the control triangular waveform enabled a one-to-one mapping between the measured RF phase (or power) and the control dc voltages. Therefore, the control voltage changes by $2V_\pi$ for a period of 25 ms.

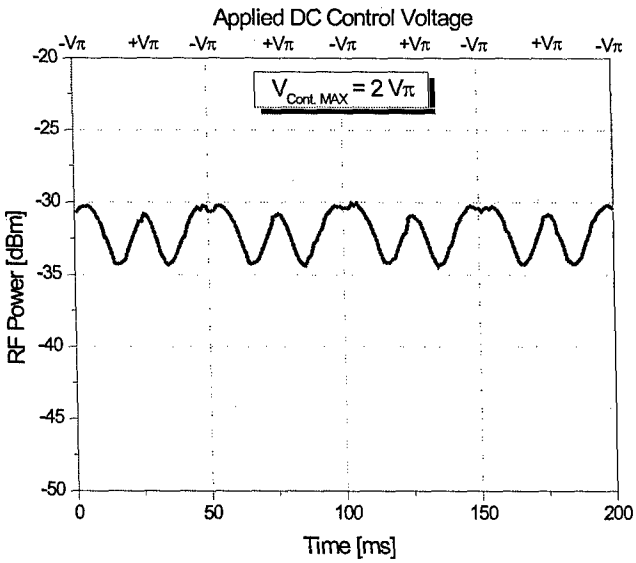

Fig. 8. The measured RF power from a single output.

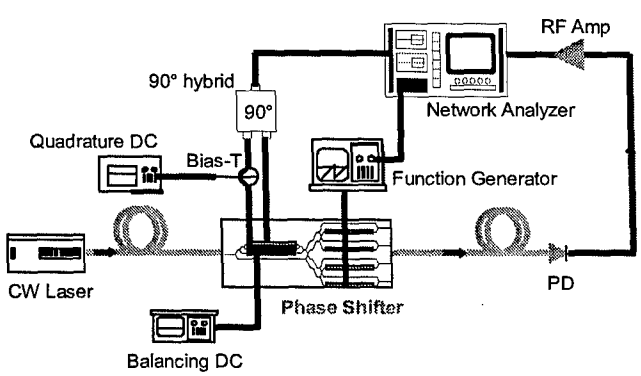

Fig. 9. The schematic diagram for the measurement setup.

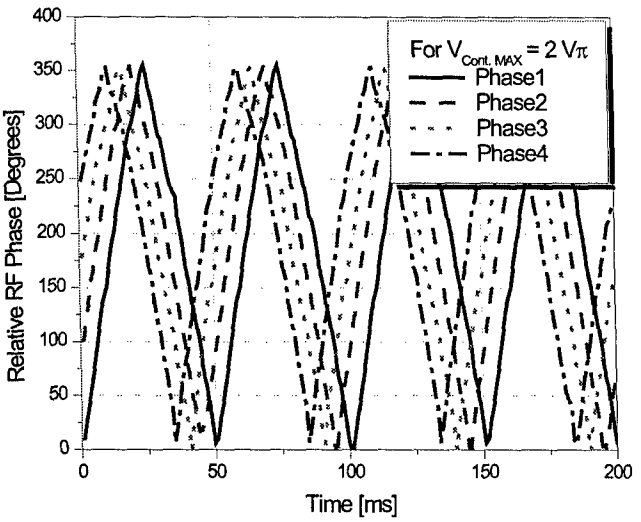

Fig. 10. The independently controlled four phase outputs introduced by equal delays on the triangular control voltages.

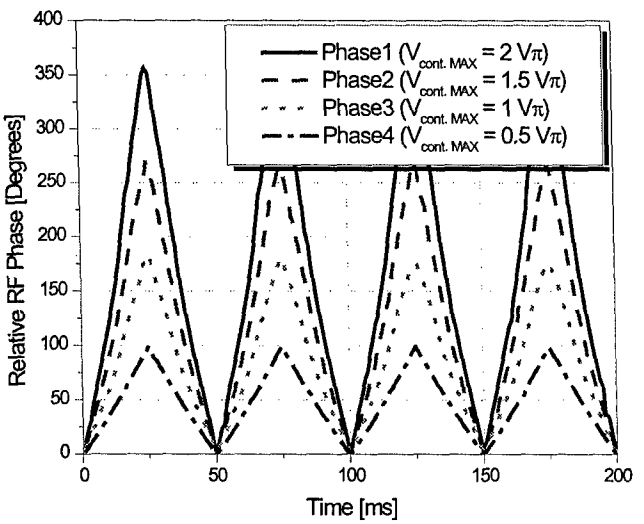

Fig. 11. The independently controlled four phase outputs introduced by the different triangular control voltages.

For the control triangular waveforms of $2V_\pi(-12V \sim +12V)$, the RF phase was tuned by 360° with a high level of linearity, and the RF power varied by less than 4 dB, as expected from Figs. 2 and 3. Note that a single control of 360° of the RF phase shift corresponds to the half-cycle of the voltage change in triangular waveforms in time domain (25 ms). Accordingly, Figs. 7 and 8 represent eight times full operation within 200 ms. This performance can be even further improved by employing the design with the optional splitting ratio of the balancing arm, as described before.

These RF phase shifters should contain the most important feature that the RF phases of an array element are independently controlled. In order to confirm this, four triangular waveforms of $2V_\pi$, set by the equal time delays, were applied to the four dc control arms. The measured RF phase characteristics are shown in Fig. 10. Almost identical characteristics having the phase shift of 360° were observed for all output ports. It can be also seen from Fig. 10 that, at a given time frame, this arrangement results in the same effect generated by four different voltages and consequently introduces the independent phase shifts at four output ports. In addition, the independent control of the RF phase was also demonstrated by applying the triangular waveforms having different peak-to-peak voltages to each control arm (Fig. 11).

The new generation of phase shifter is currently being developed, which can even reduce the complexity and drift from applying additional dc biases. Instead of using normal Y-junction splitting structures, two asymmetrical 1-by-2 MMI couplers can be used in front of the SSB modulator and the balancing arm, as shown in Fig. 12. These couplers will have multiple outputs and controllable phases depending upon their lengths and separations. This eventually will offer the built-in biases for the required optical phase shifts, removing the need for the quadrature dc biases of $V_{\pi/2}$ and V_{Bal}. Test devices of these MMI couplers were fabricated and measured. They showed the capability to provide the desired phases at two output ports. Therefore, these MMI integrated photonic RF phase shifters are expected to allow the simpler operation requiring only an RF feeding and control dc biases.

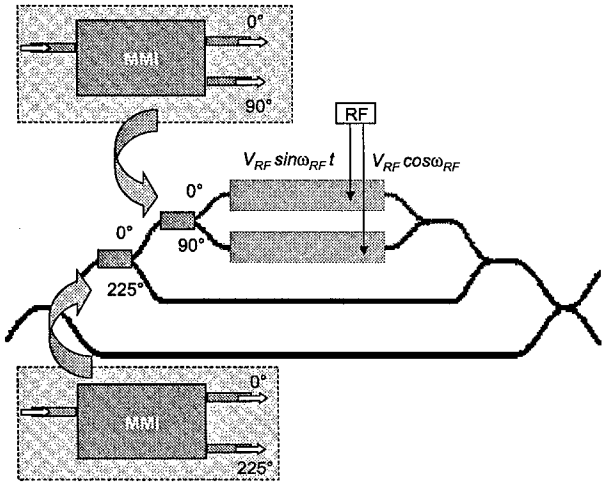

Fig. 12. The realization of the new generation of phase shifter structure incorporating MMI couplers.

IV. Conclusion

We have demonstrated a polymer-based four-element photonic RF phase-shifter array in a single chip. By employing a novel design to remove the operational drawbacks of this type of device, four phase outputs were independently controlled with high linearity and negligible power fluctuation. A simple vertical stack of these devices can now be used to form an $N \times N$ photonic RF phase shifter array without increasing complexity that will contribute to the future photonic phased array systems.

Acknowledgment

The authors would like to thank Dr. H. Erlig for valuable discussions.

References

[1] D. K. Paul, "Optical beam-forming and steering for phased-array antenna," in *Proc. IEEE Natural Telesys. Conf.*, June 1993, pp. 7–12.

[2] Y. Kamiya, W. Chujo, K. Yasukawa, K. Matsumoto, M. Izutsu, and T. Sueta, "Fiber optic array antenna using optical waveguide structure," in *IEEE Int. Symp. Dig. Antennas Propagation*, vol. 2072, May 1990, pp. 774–777.

[3] J. F. Coward, T. K. Yee, C. H. Chalfant, and P. H. Chang, "A photonic integrated-optic RF phase shifter for phased array antenna beam-forming application," *J. Lightwave Technol.*, vol. 11, pp. 2201–2205, Dec 1993.

[4] D. Jez, K. Cearns, and P. Jessop, "Optical waveguide components for beam forming in phased-array antennas," *Microwave Optical Technol. Lett.*, vol. 15, no. 1, pp. 46–49, 1997.

[5] J. M. Fuster, J. Marti, J. L. Corral, and P. Candelas, "Harmonic up/down-conversion through photonic RF phase shifters in phased-array antenna beam-forming applications," *Microwave Optical Technol. Lett.*, vol. 22, no. 4, pp. 247–249, Aug. 1999.

[6] S. R. Henion and P. A. Schulz, "Electrooptic phased array transmitter," *IEEE Photon. Technol. Lett.*, vol. 10, pp. 424–426, Mar. 1998.

[7] J. Han, H. Erlig, D. Chang, M. Oh, H. Zhang, C. Zhang, W. Steier, and H. Fetterman, "Multiple output photonic RF phase shifter using a novel polymer technology," *IEEE Photon. Technol. Lett.*, vol. 14, pp. 531–533, Apr. 2002.

[8] M. Oh, H. Zhang, A. Szep, V. Chuyanov, W. Steier, C. Zhang, L. Dalton, H. Erlig, B. Tsap, and H. Fetterman, "Electro-optic polymer modulators for 1.55 mm wavelength using phenyltetraene bridge chromophore in polycarbonate," *Appl. Phys. Lett.*, vol. 76, no. 24, pp. 3525–3527, 2000.

[9] S. Kim, H. Zhang, D. Chang, C. Zhang, C. Wang, W. Steier, and H. Fetterman, "Eelectrooptic polymer modulators with an inverted-rib waveguide structure," *IEEE Photon. Technol. Lett.*, vol. 15, pp. 218–220, Feb 2003.

[10] H. Nishihara, M. Harura, and T. Shhara, *Optical Integrated Circuits*. New York: McGraw-Hill, 1989.

Jeehoon Han (SM'01) received the B.S. degree in physics from Chonbuk National University, Chonju, Korea, in 1996 and the M.S. degree in electrical engineering from the University of Florida, Gainesville, in 1998. He is currently pursuing the Ph.D. degree in electrical engineering at the University of California, Los Angeles.

His work was on the fabrication of semiconductor laser devices. His current research is in the area of optoelectronic devices and optical communications using millimeter waves.

Byoung-Joon Seo received the B.S. degree in electrical engineering from Seoul National University, Seoul, Korea, in 1998. He is currently pursuing the M.S. degree at the University of California, Los Angeles.

He was with Woori Technology, Seoul, from 1998 to 2001.

SeongKu Kim was born on January 10, 1966, in KwangJu, Korea. He received the B.S. degree in electronics from the Chosun University, KwangJu, in 1989 and the M.S. and Ph.D. degrees in electrical engineering from Chonnam National University, KwangJu, in 1992 and 1996, respectively.

From 1994 to 1999, he was a Research Engineer with Korea Electronics Technology Institute, Seoul, Korea, where he developed the high-speed $LiNbO_3$ optical intensity modulators with a low optical loss and driving voltage. Since 2000, he has joined research programs in electrical engineering at the University of California, Los Angeles, where he initiated several projects involving the development of high-speed electrooptic polymer modulators and switches. His research interests are centered on high-speed fiber-optic communication devices, including electrooptic polymer and $LiNbO_3$ modulators and switches and their applications.

Hua Zhang, photograph and biography not available at the time of publication.

Harold R. Fetterman received the B.A. degree (with honors) from Brandeis University, Waltham, MA, in 1962 and the Ph.D. degree from Cornell University, Ithaca, NY, in 1968, both in physics.

He joined Lincoln Laboratory in 1969, where his initial research concentrated on the use of submillimeter sources for spectroscopy. In 1982, he joined the Electrical Engineering Department of the University of California, Los Angeles, as a Professor and served as the first Director of the Center for High Frequency Electronics. He has concentrated on combining high-frequency structures and systems with optical devices. These efforts include continuous-wave optical mixing experiments using three terminal devices, high-speed polymer optical modulators, and traveling-wave photodetectors, which are now being extended to over 200 GHz. Some of these devices have been incorporated into novel systems such as optically controlled phased array radars and, more recently, new forms of optical A-to-Ds.

Reduction of Fiber Chromatic Dispersion Effects in Fiber-Wireless and Photonic Time-Stretching System Using Polymer Modulators

Jeehoon Han, *Student Member, IEEE*, Byoung-Joon Seo, *Student Member, IEEE*, Yan Han, Bahram Jalali, and Harold R. Fetterman, *Fellow, IEEE, Fellow, OSA*

***Abstract*—We have investigated the general characteristics of the power penalty due to the fiber chromatic dispersion effects in both fiber-wireless and photonic time-stretching systems. Two different modulation schemes have been demonstrated to reduce this penalty using our novel polymer modulators incorporating a multimode interference (MMI) structure. A single-sideband (SSB) modulator configuration has almost completely eliminated this penalty without a bandwidth limit. A double-sideband (DSB) modulator configuration with an appropriate quadrature bias has also shown significant improvement in bandwidth limitations for a given fiber link length.**

***Index Terms*—Fiber-wireless systems, photonic time-stretching, polymer modulators, power penalty, single-sideband modulation.**

I. Introduction

IN FIBER-WIRELESS systems, the radio frequency (RF) signals are generated at the central exchange using optical techniques and transmitted to the remote base stations over optical fiber links. The simplest and best technique to modulate optical fields with RF signals is an intensity modulation scheme via Mach–Zehnder modulators (MZMs) with continuous-wave (CW) lasers. Using the conventional DSB modulation scheme, the RF power detected at the base station suffers from a periodic degradation due to the fiber chromatic dispersion. As the RF frequency or fiber-link distance increases, this effect is even more severe and limits the system performance. This detrimental effect can be mitigated using alternative modulation schemes [1]–[3]. In this paper, we derive more specific and standard expressions and confirmed them by experiments using standard MZM designs. This examination of the power penalty in CW applications can be also utilized for the appropriate and clear understanding of those in pulsed applications.

Photonic time-stretching (PTS) utilizes optical systems to enable high-speed analog-to-digital conversion (ADC) of RF signals at otherwise inaccessible high frequencies. By exploiting chirped optical pulses and chromatic dispersion in standard optical fibers, high-frequency RF signals can be stretched in time, without distortion, to lower frequency regimes where conventional electronic ADCs are able to digitize with high resolution. However, as in CW applications, the inherent fiber chromatic dispersion effects limit the actual bandwidth of PTS system [4]–[6]. We describe the general theory and present for the first time the experimental demonstration of PTS system associated with various modulation conditions including SSB modulation.

Manuscript received October 11, 2002; revised February 27, 2003. This work was supported in part by AFOSR and DARPA.

The authors are with the Electrical Engineering Department, University of California, Los Angeles, CA 90095 USA (e-mail: hoon@ ee.ucla.edu).

Digital Object Identifier 10.1109/JLT.2003.812155

II. Power Penalty in Fiber-Wireless System

The basic structure for these MZMs is shown in Fig. 1 representing all possible modulation schemes and biases. If the input optical signal at Ω is $E_{\text{in}}(t) = e^{i\Omega t}$ with unit magnitude, the generalized expression for output optical field from MZM modulated at ω_m is given by

$$E(t) = \frac{1}{2} e^{i\Omega t} \left\{ e^{i\Delta_1 \cos(\omega_m t + \theta)} + e^{i\Delta_2 \cos(\omega_m t) + i\phi_b} \right\} \quad (1)$$

where $\Delta_i = \pi V_i / V_\pi$ is the modulation depth at i arm, $\phi_b = \pi V_b / V_\pi$ is the optical phase shift controlled by dc bias, V_π is the half-wave voltage. When this signal travels through the standard fiber with length of L, the resulting optical field can be written in terms of three frequency components, Ω, $\Omega - \omega_m$ and $\Omega + \omega_m$, with different phase changes due to the chromatic dispersion

$$\begin{aligned} E(t, L) = \frac{1}{2} \Big\{ & \left[J_0(\Delta_1) + J_0(\Delta_2) e^{i\varphi_b} \right] e^{i\Omega t} e^{-i\varphi_\Omega} \\ & + i \left[J_1(\Delta_1) e^{-i\theta} + J_1(\Delta_2) e^{i\varphi_b} \right] \\ & \times e^{i(\Omega - \omega_m)} e^{-i\varphi_{\Omega - \omega_m}} \\ & + i \left[J_1(\Delta_1) e^{i\theta} + J_1(\Delta_2) e^{i\varphi_b} \right] \\ & \times e^{i(\Omega + \omega_m)} e^{-i\varphi_{\Omega + \omega_m}} \Big\} \end{aligned} \quad (2)$$

where $J_0(\Delta_1)$, $J_0(\Delta_2)$, $J_1(\Delta_1)$, $J_1(\Delta_2)$ are the Bessel function values and Δ is assumed to be small. Each phase change can be specified by usual Taylor expansion of the propagation constants $\beta(\omega)$

$$\begin{aligned} \varphi_\Omega &= \beta(\Omega) L \\ \varphi_{\Omega - \omega_m} &= \beta(\Omega) L - \beta'(\Omega) L \omega_m + \frac{1}{2} \beta''(\Omega) L \omega_m{}^2 \\ \varphi_{\Omega + \omega_m} &= \beta(\Omega) L + \beta'(\Omega) L \omega_m + \frac{1}{2} \beta''(\Omega) L \omega_m{}^2 \end{aligned} \quad (3)$$

where group velocity dispersion in standard fibers is defined by $D_\lambda = |2\pi c \beta'' / \lambda_0{}^2| = 17$ ps/km · nm.

At the photodiode, the RF signal at modulation frequency is produced as a result of interference among these components. Normally the detected RF power is associated with their phase

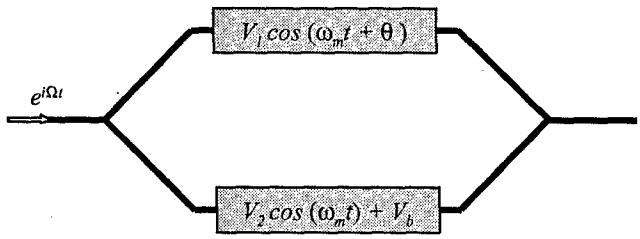

Fig. 1. The general schematic for MZM structure representing all possible modulation schemes and bias conditions.

relationship, which consequently is a strong function of the dispersion parameter, fiber length and modulation frequency as can be seen in (3). In the following sections, it will be shown that it also could be significantly affected by modulation schemes and bias conditions.

A. Push–Pull DSB Modulation ($\Delta_1 = \Delta_2 = \Delta$, $\theta = \pi$)

Both arms are driven by RF signals with equal power and out of phase by π. One arm is biased either at V_{+b} or V_{-b} corresponding to the quadrature bias voltages on the positive or negative slope of the MZM transfer function such that $\phi_{+b} = \pi V_{+b}/V_\pi = \pi/2$, $\phi_{-b} = \pi V_{-b}/V_\pi = -\pi/2$ with respect to the other arm. This is so called push-pull operation and the optical field from the MZM can be expressed by

$$E(t) = \frac{1}{2} e^{i\Omega t} \left\{ e^{-i\Delta \cos(\omega_m t)} \pm i e^{i\Delta \cos(\omega_m t)} \right\} \quad (4)$$

The resulting intensity at the modulation frequency after propagating through fiber of length L is

$$I_{\omega_m}(t) \propto J_0 J_1 \cos\left(\frac{\beta'' L \omega_m{}^2}{2}\right) \cos(\omega_m t - \beta' L \omega_m). \quad (5)$$

An optical carrier and two sidebands generated by DSB modulation experience different phase shifts along the fiber and result in a relative phase difference between the carrier and each sideband. Due to this effect, the RF power detected at the modulation frequency is not constant but varies with their phase relationship, which is dependent on dispersion parameter, fiber length, and modulation frequency. This power penalty is represented by the first cosine term in (5). Since, in this case, both RF arms are balanced, there is no initial phase difference between carrier and each sideband at the MZM so that the power variation appears in the form of $\cos((\beta'' L \omega_m{}^2)/2)$for both quadrature biases.

B. Single-Arm DSB Modulation ($\Delta_1 = 0$, $\Delta_2 = \Delta$)

When only one of arms is modulated and biased at $V_{\pm b}$, the optical field from the MZM can be expressed by

$$E(t) = \frac{1}{2} e^{i\Omega t} \left\{ 1 \pm i e^{i\Delta \cos(\omega_m t)} \right\} \quad (6)$$

The resulting intensity at ω_m after propagating through fiber of length L is

$$I_{\omega_m}(t) \propto J_0 J_1 \cos\left(\frac{\beta'' L \omega_m{}^2}{2} \pm \frac{\pi}{4}\right) \cos(\omega_m t - \beta' L \omega_m). \quad (7)$$

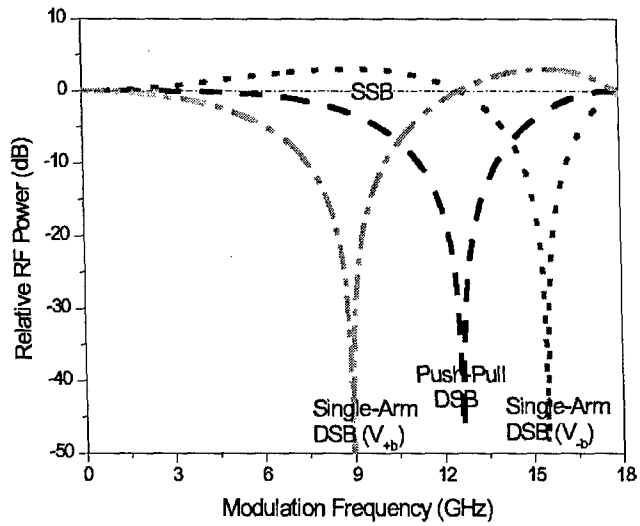

Fig. 2. Power penalty as a function of modulation frequencies in CW system with different modulation schemes and quadrature biases for length of 23 km.

Similar to the previous push-pull operation case, the detected RF power is varying with the cosine function (first cosine term) due to the same effect. However, in this case, this modulation scheme introduces the additional phase difference between the carrier and each sideband at the MZM, which influences the detected RF power. As shown in (7), the first cosine term is shifted by $\pm\pi/4$ when the signs correspond to quadrature bias voltages, $V_{\pm b}$. This indicates that the power nulls for the two different quadrature biases appear at different modulation frequencies (or fiber lengths). The DSB modulation driven in this fashion can increase the bandwidth for a given fiber link length or vice versa.

Fig. 2 shows the theoretical graph for the power penalty as a function of modulation frequencies resulting from the two DSB modulation schemes discussed above. Push-pull operation has only one power null while single-arm operation has two depending on the quadrature bias points as shown in Fig. 2. It can be also seen that single-arm operation biased at V_{-b} provides enhanced bandwidth compared to other two moulation schemes. On the other hand, even though the same modulation scheme is applied, the bandwidth is degraded by a factor of $\sqrt{3}$ when biased at V_{+b}.

C. SSB Modulation ($\Delta_1 = \Delta_2 = \Delta$, $\theta = \pm\pi/2$)

When the both arms are modulated but the RF phase difference on the two arms is $\pm\pi/2$, with quadrature bias voltage $V_{\pm b}$, the optical field from the MZM becomes

$$E(t) = \frac{1}{2} e^{i\Omega t} \left\{ e^{\mp i\Delta \sin(\omega_m t)} \pm i e^{i\Delta \cos(\omega_m t)} \right\}. \quad (8)$$

The resulting intensity at ω_m after propagating through fiber L is

$$I_{\omega_m}(t) \propto J_0 J_1 \sin\left(\omega_m t - \beta' L \omega_m \pm \frac{\pi}{4}\right). \quad (9)$$

The SSB modulation cancels out one of the sidebands and generates only one sideband with a carrier. As a consequence, it is seen in (9) that the first cosine term associated with the power penalty disappears so that detected RF power is constant.

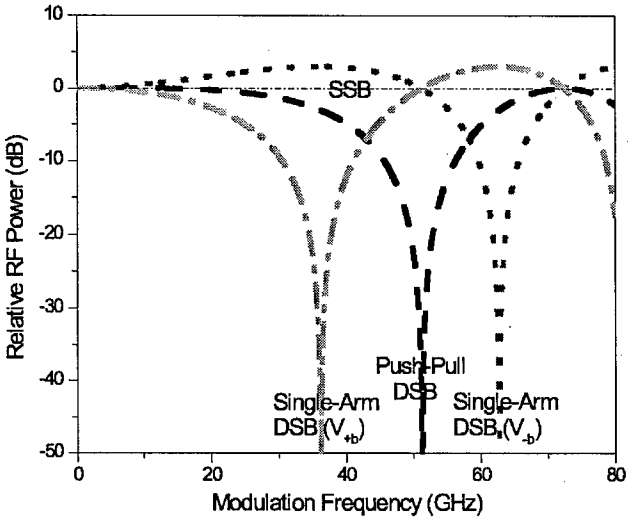

Fig. 3. Theoretical power penalty in PTS system with various modulation schemes and quadrature biases for M = 10.

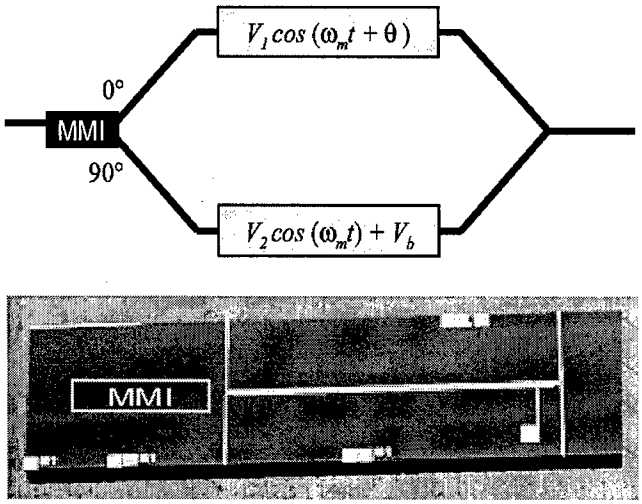

Fig. 4. MZMs incorporating MMI couplers and devices fabricated with polymer material, CPW1/APC.

Ideally, the RF signal generated by SSB modulation does not suffer from bandwidth or fiber link length limitations with either quadrature bias (see Fig. 2).

III. Power Penalty in Time-Stretching System

PTS systems exploit the group velocity dispersion to temporally expand a pulse while preserving its envelope shape which has information. The details of this theory are described in [4]–[6]. Instead of the plane waveform in the CW case, a transform limited Gaussian pulse is assumed such as

$$E_{\text{source}}(t) = \exp\left(-\frac{t^2}{\tau^2}\right)\exp(i\Omega t). \tag{10}$$

Then, the same principle as in the CW system is applied to the PTS system so that the resulting intensity at ω_m for each modulation scheme is

$$I_{\omega_m}(t) \propto \cos\left(\frac{\beta'' L_2 {\omega_m}^2}{2M}\right): \text{push-pull DSB with } V_{\pm b} \tag{11}$$

$$I_{\omega_m}(t) \propto \cos\left(\frac{\beta'' L_2 {\omega_m}^2}{2M} \pm \frac{\pi}{4}\right): \text{single-arm DSB with } V_{\pm b} \tag{12}$$

$$I_{\omega_m}(t) = const: \text{SSB with } V_{\pm b} \tag{13}$$

where a stretching factor $M = 1 + (L_2/L_1)$.

Fig. 3 shows the theoretical graph for the power penalty as a function of modulation frequencies in a PTS system with $M = 10$. In the SSB modulation, the cosine term associated with power penalty disappears so that detected RF power is constant and does not suffer from bandwidth or fiber link length limitations with either quadrature bias. As in the CW case, push-pull operation has only one power null while single-arm operation has two depending on the quadrature bias points. For example, when the PTS system incorporates either SSB modulation or single-arm DSB modulation biased at V_{-b}, RF signals of up to 40 GHz (which is attainable by current technology) can be stretched out up to 4 GHz with $M = 10$ without suffering from the power penalty. On the other hand, the power degradation is severe for push-pull operation or single-arm operation biased at V_{+b} in this modulation frequency range.

IV. Device Fabrication and Experimental Setup

The SSB MZM structure in Fig. 4 was fabricated using the recently developed polymer materials (CPW1/APC) and advanced polymer fabrication technologies. This guest-host system exhibits a high EO coefficient, low material loss at 1.55 μm, and wideband frequency response over 100 GHz [7]. The single mode (SM) ridge optical waveguides were fabricated using the new inverted rib structures [8]. The key benefit of these inverted rib structures is that it can eliminate the damage problem on the core layer by the photoresist solvents when the waveguides are defined in the core layer. This ultimately resulted in much simpler fabrication procedure and lower propagation losses. Also the SM waveguide structures were designed to provide the symmetric mode shape with a rib depth of 0.8 μm and waveguide width of 4 μm. A large optical nonlinearity in the core region was achieved through electrode poling. The microstrip lines were vertically aligned to the optical waveguides in the interaction regions to provide inherent velocity match of RF signal and optical signal.

In order to reduce the complexity and bias drift from applying additional DC bias, instead of using a normal Y-junction splitting structure, an asymmetrical 1-by-2 MMI coupler was used in front of the SSB modulator. This structure was intended to offer the built-in bias with the equal power and required optical phase shifts of $\pi/2$ for two arms. The measured excess loss due to the MMI was less than 1 dB and power difference at two outputs was less than 0.1 dB, which corresponds to the phase difference less than 1°.

Fig. 5 shows the experimental setup for the PTS system (and CW system). The optical source is a passively mode-locked Er^{3+} fiber pulse laser with a 40 nm bandwidth at 1.55 μm and a 40 MHz repetition rate (1.55 μm Er^{3+} fiber CW laser for CW system). Both fiber spools L_1 and L_2 are standard SMF ($L_1 = 0$, $L_2 = 23$ km for CW system). The dispersed input optical signal from L_1 is modulated at MZM by a 20 GHz sweep

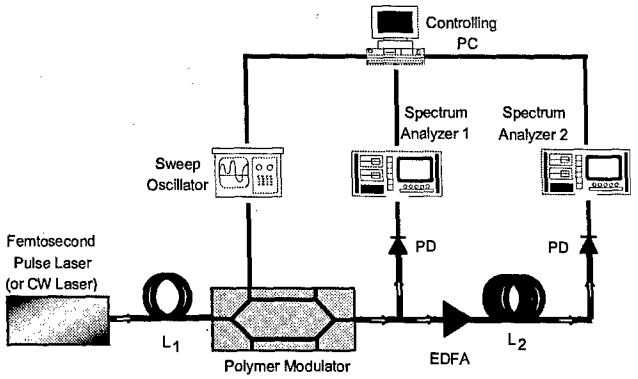

Fig. 5. Block diagram of experimental setup for PTS system (or CW system).

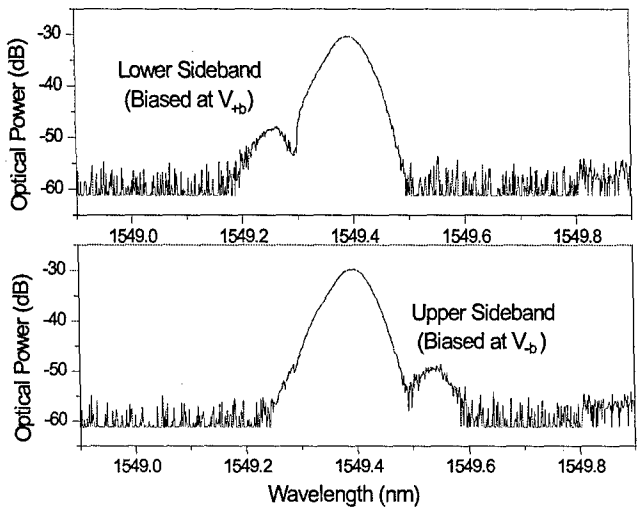

Fig. 6. Measured optical output SSB spectrums on OSA at a modulation frequency of 18 GHz.

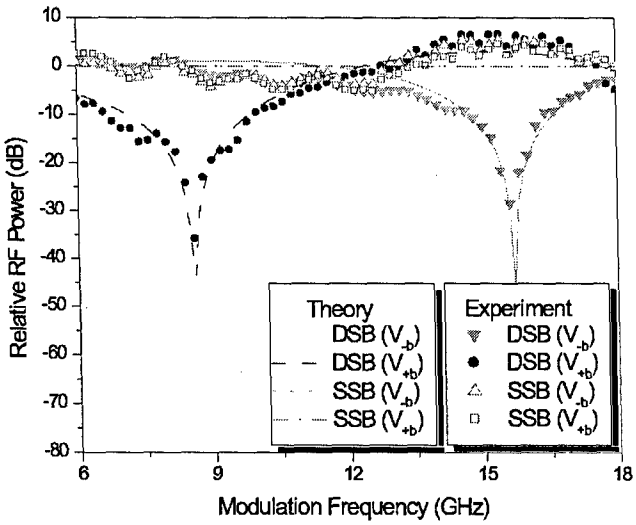

Fig. 7. Measured power penalty in CW system for various modulation schemes and quadrature biases ($L = 23$ km).

oscillator and amplified in an EDFA before entering L_2. The stretched output from L_2 spool is detected by a photodiode and amplified by a RF amplifier. To exclude the frequency response of the MZM, the difference of the RF power before and after L_2 is measured by two RF spectrum analyzers.

V. Experimental Results

A. Measurement in CW System

The SSB modulation at 18 GHz with a CW laser was first confirmed on the optical spectrum analyzer (OSA) at both quadrature bias voltages $V_{\pm b}$ to ensure the performance of our SSB modulators (Fig. 6). The upper sideband spectrum is corresponding to the quadrature bias at V_{-b}, and lower upper sideband spectrum is corresponding to the quadrature bias at V_{+b}.

Fig. 7 shows the measured power penalty for the various modulation schemes and two quadrature bias points when the fiber length is 23 km. For the SSB modulation, the power nulls have not been observed for the entire frequency range at both quadrature bias points. On the other hand, the DSB modulation driven by single-arm operation has different power nulls depending on the quadrature bias points. The bandwidth, when biased at V_{-b}, has been increased by an amount of $\sqrt{3}$ compared to the other quadrature bias point as can be seen in (7). The measured power nulls corresponding to V_{+b} and V_{-b} appear at 8.6 GHz and 15.6 GHz, respectively, slightly deviates from the expected values from (7) by approximately 0.5 GHz. This can be caused by factors such as an uneven splitting ratio, the modulation depth and small deviations from the quadrature bias points. These factors cause a small change in the initial phase which can slightly move the positions of the power nulls. The theoretical plot in Fig. 7 is calculated assuming a splitting ratio of 1, a negligible modulation depth ($J_0 = 1$) and a deviation from the quadrature bias of 0.3 V.

B. Measurement in PTS System

In our PTS measurement, the RF signal of up to 18 GHz was stretched out to 8.6 GHz ($M = 2.1$). At each modulation frequency, the center of the shifted RF spectrum is observed on the spectrum analyzer. Fig. 8 shows the measured output RF frequencies as a function of modulation frequencies with fiber spools, $L_1 = 13.5$ km and $L_2 = 15$ km, which is in good agreement with the theoretical value for all modulation schemes and bias conditions. A low M factor of 2.1 was intentionally used in our experiment to be able to see the first power nulls resulting from the DSB modulation biased at $V_{\pm b}$ below 20 GHz frequency range. Since the frequency values at power nulls are proportional to $\sqrt{M}$, the first power nulls for the M greater than 2 appear far beyond this frequency range.

The measured RF power penalties as a function of modulation frequency for the various modulation conditions are shown in Fig. 9. Also shown in Fig. 9 are the theoretical power penalties including the effects described in the CW case such as a splitting ratio of 0.95, a negligible modulation depth ($J_0 = 1$) and a deviation from the quadrature bias of 1.3 V. The deviation from the original theoretical plot without considering these effects is about 2.5 GHz.

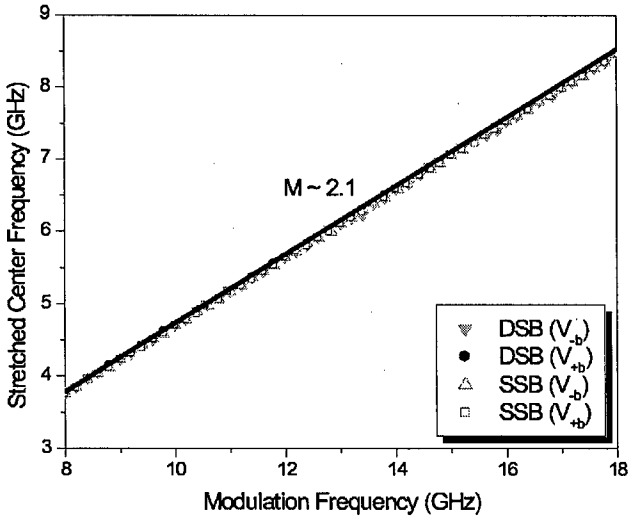

Fig. 8. Measured time stretch ratio for DSB and SSB modulation with different quadrature biases.

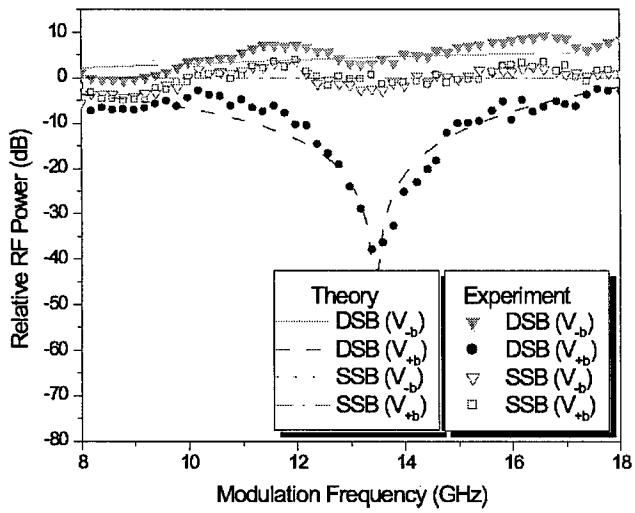

Fig. 9. Measured power penalty in PTS system for various modulation schemes and quadrature biases.

The DSB modulation biased at V_{+b} shows the first power null at around 13.5 GHz while the DSB modulation biased at V_{-b} is expected to appear at 28 GHz. Therefore, the limit on the modulation frequency can be significantly improved even for the DSB modulation by using the alternative quadrature bias point. On the other hand, the SSB modulation, for both quadrature bias points, almost completely eliminates this penalty effect without a bandwidth limit as shown in Fig. 9.

Fig. 10 shows the RF power spectral density of modulated pulse before and after stretching for the DSB modulation with two quadrature bias points, $V_{\pm b}$, at the modulation frequency of 13.5 GHz. As expected from Fig. 9, the stretched RF signals at this modulation frequency exhibit considerable amount of power at quadrature bias point V_{-b} and almost zero power at quadrature bias point V_{+b}.

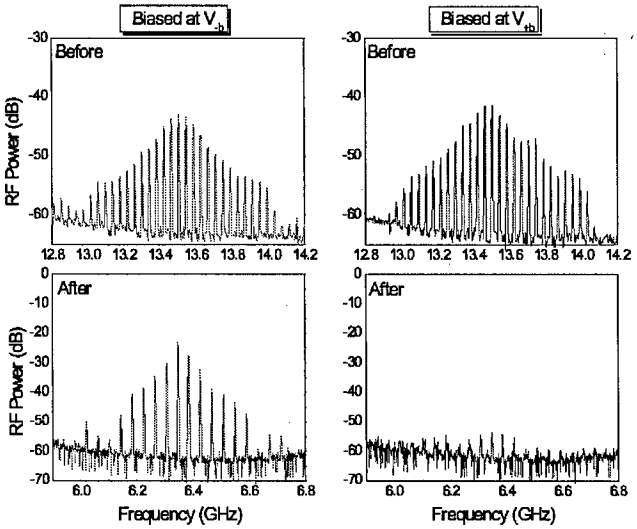

Fig. 10. RF power spectral density of modulated pulse before and after stretching for DSB modulation at two quadrature bias points. The spacing between peaks corresponds to the repetition rate of the mode-locked laser.

VI. Conclusion

In both fiber wireless and photonic time-stretching system, the power penalty due to the fiber chromatic dispersion effects is undesirable and limits the system performance. We have demonstrated techniques to reduce this power penalty using both polymer-based SSB and DSB modulators. The limit on the modulation frequency due to this penalty can be almost completely eliminated with the SSB modulation without a bandwidth limitation and also can be significantly improved with the DSB modulation by using an alternative quadrature bias point. These results indicate that SSB modulation or appropriately biased DSB modulation can have important roles in both CW and pulsed applications.

References

[1] A. Gnauck, S. Korothy, J. Veselka, J. Nagel, and D. Moser, "Dispersion penalty reduction using an optical modulator with adjustable chirp," *IEEE Photon. Technol. Lett.*, vol. 3, pp. 916–918, Oct. 1991.

[2] F. Devaux, Y. Sorel, and J. Kerdiles, "Simple measurement of fiber dispersion and of chirp parameter of intensity modulated light emitter," *J. Lightwave Technol.*, vol. 11, pp. 1937–1940, Dec. 1993.

[3] G. Smith, D. Novak, and Z. Ahmed, "Overcoming chromatic-dispersion effects in fiber-wireless systems incorporating external modulators," *IEEE Trans. Microwave Theory Tech.*, vol. 45, pp. 1410–1415, Aug. 1997.

[4] F. Coppinger, A. Bhushan, and B. Jalali, "Photonic time stretch and its application to analog-to-digital conversion," *IEEE Trans. Microwave Theory Tech.*, vol. 47, pp. 1309–1314, July 1999.

[5] D. Chang, H. Erlig, M. Oh, C. Zhang, W. Steier, L. Dalton, and H. Fetterman, "Time stretching of 102-GHz millimeter waves using novel 1.55 um polymer electrooptic modulator," *IEEE Photon. Technol. Lett.*, vol. 12, pp. 537–539, May 2000.

[6] J. Fuster, "Single-sideband modulation in photonic time-stretch analog-to-digital conversion," *Electron. Lett.*, vol. 37, no. 1, pp. 67–68, Jan 2001.

[7] M. Oh, H. Zhang, C. Zhang, H. Erlig, Y. Chang, B. Tsap, D. Chang, A. Szep, W. Steier, H. Fetterman, and L. R. Dalton, "Recent advances in electrooptic polymer modulators incorporating highly nonlinear chromophore," *IEEE J. Select. Topics Quantum Electron.*, vol. 7, pp. 826–835, Sept./Oct. 2000.

[8] S. Kim, H. Zhang, D. Chang, C. Zhang, C. Wang, W. Steier, and H. Fetterman, "Electrooptic polymer modulators with an inverted-rib waveguide structure," *IEEE Photon. Technol. Lett.*, vol. 15, pp. 218–220, Feb. 2003.

Jeehoon Han (S'01) received the B.S. degree in physics from the Chonbuk National University, Chonju, South Korea, in 1996 and the M.S. degree in electrical engineering from the University of Florida, Gainesville, in 1998, working on the fabrication of semiconductor laser devices. He is currently pursuing the Ph.D. degree in electrical engineering at the University of California, Los Angeles.

His current research is in the area of optoelectronic devices and optical communications using millimeter waves.

Byoung-Joon Seo (S'03) received the B.S. degree in electrical engineering from Seoul National University, Seoul, Korea, in 1998 and worked for Woori Technology in Seoul, from 1998 to 2001. He is currently pursuing the M.S. degree at the University of California, Los Angeles.

Yan Han received the B.S. and M.S. degrees in electronic engineering from the Tsinghua University at Beijing, China, in 1998 and 2000, respectively. He is currently a doctoral candidate in the Department of Electrical Engineering at the University of California, Los Angeles.

His research interests include the areas of microwave photonic systems, optical communication systems, wireless communication systems, optical amplifiers, and fiber optics.

Bahram Jalali is a Professor of Electrical Engineering, the Director of the DARPA Center for Optical A/D System Technology (COAST) and the Director of the Optoelectronic Circuits and System Laboratory at University of California, Los Angeles (UCLA).

From 1988 to 1992, he was a Member of Technical Staff at the Physics Research Division of AT&T Bell Laboratories in Murray Hill, NJ, where he conducted research on ultrafast electronics and optoelectronics. He was responsible for successful development and delivery of 10 Gb/s lightwave circuits to U.S. Air Force in 1992. His current research interests are in microwave photonics, integrated optics, and fiber-optic ICs. He has over 100 publications and holds five U.S. patents. He a member of the California Nano Sciences Institute (CNSI) and serves on the Advisory Board of the Discovery Center for Science and Technology, a southern California nonprofit organization. While on leave from UCLA from 1999 to 2001, he founded Cognet Microsystems, a Los Angeles-based fiber-optic component company. He served as Cognet's President, CEO, and Chairman, until the company's acquisition by Intel Corporation in April 2001.

Dr. Jalali was awarded the BridgeGate 20 Award in recognition of his contributions to the southern California high tech economy.

Harold R. Fetterman (SM'81–F'90) received the B.A. degree with honors from Brandeis University, Waltham, MA, and the Ph.D. degree in physics from Cornell University, Ithaca, NY, in 1962 and 1968, respectively.

Dr. Fetterman joined Lincoln Laboratory, Lexington, MA, in 1969, where his initial research concentrated on the use of submillimeter sources for spectroscopy. Since leaving Lincoln Laboratory, he has devoted his efforts to investigating new solid-state devices. During this period, he was one of the founders of the highly respected Millitech Corporation. In 1982, he joined the University of California, Los Angeles (UCLA), Electrical Engineering Department as a Professor and served as the first Director of the Center for High Frequency Electronics. From 1986 to 1989, he was Associate Dean for Research in the School of Engineering. Currently, he has programs in investigating new millimeter wave device concepts and novel means of high frequency testing using laser techniques. He has concentrated on combining high frequency structures and systems with optical devices. These efforts include CW optical mixing experiments using three terminal devices, high-speed polymer optical modulators and traveling wave photodetectors which are now being extended to over 200 GHz.

Dr. Fetterman is a Fellow of the Optical Society of America (OSA) and is currently the Chair of the Executive Committee of the Henry Samueli School of Engineering and Applied Science at UCLA.

Photo-bleaching induced electro-optic polymer modulators with dual driving electrodes operating at 1.55 μm wavelength

SeongKu Kim, K. Geary, H.R. Fetterman, C. Zhang, C. Wang and W.H. Steier

Electro-optic (EO) polymeric Mach-Zehnder (MZ) modulators with photo-bleaching (PB) induced waveguides and dual driving electrodes operating at 1.55 μm wavelength have been demonstrated. The half-wave voltage of the integrated polymeric modulator was 4.5 V in a push–pull configuration with a 1.5 cm interaction length. The extinction ratio was greater than 20 dB, and the fibre-to-fibre insertion loss was 8 dB for the TM polarisation. The achieved fibre-to-fibre insertion loss and driving voltage are the best, to the authors knowledge, in the reported PB induced MZ EO polymeric modulators.

Introduction: Photo-bleaching (PB) is an attractive method for fabricating optical waveguides in polymeric material. The main advantages of the method include the ease of high quality optical waveguide fabrication and the ability to precisely tailor the index [1, 2]. So far, several passive and active devices using the PB-induced optical waveguide have been reported such as polarisers [3, 4], and modulators [5–7]. In regard to modulators developed by the PB technique, there have been limited results. In addition, the best performance [7] had a driving voltage of 9 V and fibre-to-fibre insertion loss of 13.2 dB at 1.3 μm wavelength, which are too high for today's photonic device applications. On the other hand, a reduced driving voltage of 4.5 V at 1.3 μm wavelength was reported in [6], but the fibre-to-fibre insertion loss and the extinction ratio were not mentioned clearly. To the best of our knowledge, no study on lowering the driving voltage and fibre-to-fibre insertion loss of the PB induced optical modulators has been performed, particularly operating at 1.55 μm wavelength.

In this Letter, polymeric electro-optic (EO) Mach-Zehnder (MZ) optical modulators employing PB induced waveguides in the EO polymer material 'APC-CPW1', [8–11] are demonstrated for the first time.

Experiments and results: A schematic view of the fabricated optical modulator is given in Fig. 1. The dual driving electrode design of a MZ optical modulator inherently offers the capability to adjust the phase of the voltages on the electrodes, which produces zero-chirp modulation operation [12–14].

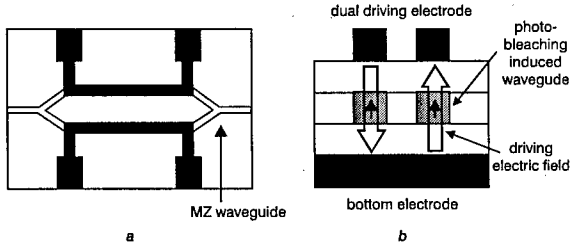

Fig. 1 *Schematic diagram of integrated PB induced EO polymer modulator with dual driving electrode*

a Top view
b Cross-sectional view

Our devices are made using the EO polymer APC-CPW1 (also known as APC-CLD1), a phenyltetraene bridged high-$\mu\beta$ guest chromophore in an amorphous polycarbonate host. The material's refractive index changes as a result of UV light irradiation at room temperature. The amount of change is a predictable function of exposure time. Using a 8 mW/cm^2 intensity light from Mask Aligner (Karl Suss MA6, USA), the change of the refractive index against exposure time is shown in Fig. 2 for TM polarisation at 1.55 μm wavelength. We have observed a large refractive index decrease with increasing bleaching time in TM polarisation (also, in TE polarisation). As a result, it was confirmed that the predominant PB mechanism in our EO material, APC-CPW, is photochemical decomposition (photoreduction) of the chromophore and not an isomerisation reaction [15]. Therefore, the unexposed region remains as a core layer and the exposed region is changed into a cladding, providing optical confinement in the lateral direction.

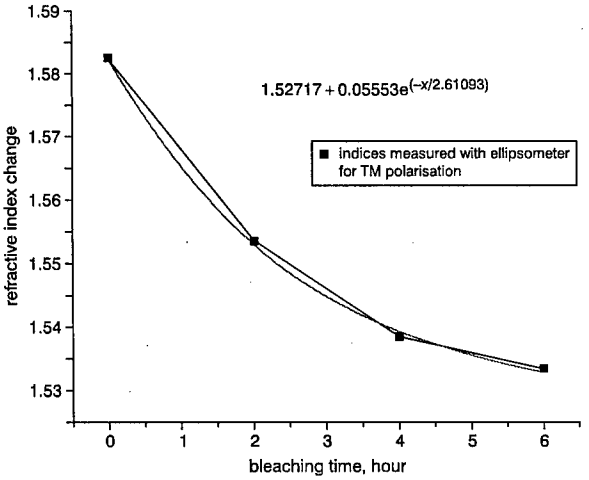

Fig. 2 *Changes in EO polymer refractive indices, APC-CPW1, at $\lambda = 1.55$ μm against PB time*

For the fabrication of the PB-induced optical modulator, a 11 wt.% solution of CPW1 was filtered via a 0.2 μm filter and spin-coated on a 2.5 μm thick UV-15LV coated Si wafer substrate. Then an upper cladding of UFC-170A was spin-coated ~2.5 μm. After that, the poling was performed at 150°C with 500 V applied voltage in a nitrogen-purged box. Then PB was performed for time periods ranging from 0 to 6 hours. Finally, the electrodes were electro-plated, increasing the electrode thickness to ~3 μm.

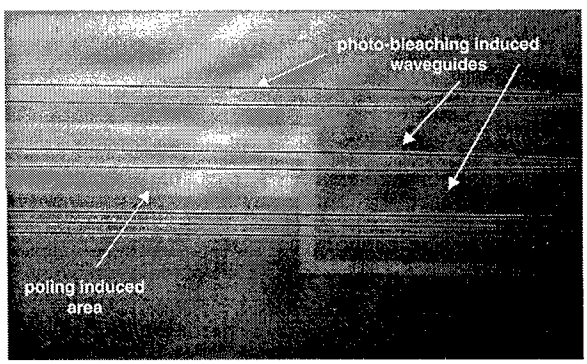

Fig. 3 *Top view of poling induced area and PB induced waveguides at near MZ waveguide section*

Optical MZ waveguide is 4 μm wide and 2.4 cm long

A photograph of the device surface near the Y-branch of two MZ waveguides is shown in Fig. 3. Two MZ waveguides were formed along with 3, 4, and 5 μm wide waveguides. Only the selected MZ waveguide (in the middle) underwent the high-voltage poling and then the PB procedure. After performing a 1 hour PB, the refractive index of both polarisations is decreased by ~0.016 as estimated in Fig. 2, resulting in an optical waveguide that supports both a TE and TM mode. The poling current was monitored to identify the induced poling current behaviour during the poling process. Previously, the poling current was set to be less than 300 nA maximum [11] to prevent possible poling-induced optical loss. In reality, how the magnitude of the poling induced current affects the poling induced loss is not clear due to fabrication factors, such as the uniformity of the guiding and cladding films introduced by various processing steps [16]. However, a peak current of less than ~5 μA in our study was observed. To identify the poling induced optical loss, we have measured the insertion loss of the unpoled and poled waveguides that were located adjacent to the MZ waveguide on the same device. As a result, there was no noticeable increase in optical

propagation loss. The near-field profile at the output end of the 4 μm wide MZ waveguide for the TM polarised mode was also observed. It was confirmed that the fabricated optical waveguides support only a single mode when the fibre position at the input port changed.

The TM mode fibre-to-fibre loss of a 4 μm wide MZ modulator was measured to be ~8 dB. The measured modulation of a fabricated device at a 1.55 μm is shown in Fig. 4. A half-wave modulation voltage of ~9 V was measured in a single driving 1.5 cm interaction length using 1 kHz triangular electrical modulation signal, implying a 4.5 V of driving voltage in a push–pull operation.

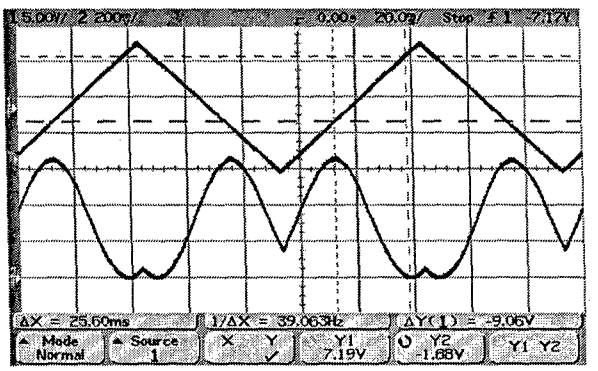

Fig. 4 *Low frequency (1 kHz) transfer function measurements at* $\lambda = 1.55$ *μm*

Single arm driving operation at $\lambda = 1.55$ μm shows $V_\pi \sim 9$ V and extinction ratio >20 dBm

Conclusion: We report a PB induced optical modulator with dual-driving electrodes. The optical waveguides created support both TE and TM polarisations with low insertion loss, which could be further reduced by optimising the PB time. The resulting device performances are comparable to that obtained in our earlier work [9, 11] developed using a ridge-type optical waveguide, and are the first results operating at 1.55 μm wavelength in reported PB induced polymer modulators.

14 June 2003
Electronics Letters Online No: 20030873
DOI: 10.1049/el:20030873

SeongKu Kim, K. Geary and H.R. Fetterman (*Department of Electrical Engineering, University of California—Los Angeles, Los Angeles, CA 90095, USA*)

E-mail: kimsku@ee.ucla.edu

C. Zhang and C. Wang (*Pacific Wave Communications, Los Angeles, CA 90024, USA*)

W.H. Steier (*Department of Electrical Engineering, University of Southern California, Los Angeles, CA 90089, USA*)

References

1 MOSHREFZADEH, R.S., MISEMER, D.K., RADCLIFFE, M.D., FRANCIS, C.V., and MOHAPATRA, S.K.: 'Nonuniform photobleaching of dyed polymers for optical waveguides', *Appl. Phys. Lett.*, 1993, **62**, (1), pp. 16–18

2 WATANABE, O., TSUCHIMORI, M., OKADA, A., and ITO, H.: 'Mode selective polymer channel waveguide defined by the photoinduced change in birefringence', *Appl. Phys. Lett.*, 1997, **71**, (6), pp. 750–752

3 LEE, S.-S., GARNER, S., CHEN, A., CHUYANOV, V., STEIER, W.H., AHN, S.-W., and SHIN, S.-Y.: 'TM-pass polarizer based on a photobleaching-induced waveguide in polymers', *IEEE Photonics Technol. Lett.*, 1998, **10**, (6), pp. 836–838

4 LEE, S.-S., AHN, S.-W., and SHIN, S.-Y.: 'Integrated optical waveguide polarizer based on photobleaching-induced birefringence in an electrooptic polymer', *IEEE Photonics Technol. Lett.*, 1997, **9**, (8), pp. 1125–1128

5 GIRTON, D.G., KWIATKOWSKI, S.L., LIPSCOMB, G.F., and LYTEL, R.S.: '20 GHz electro-optic polymer Mach-Zehnder modulator', *Appl. Phys. Lett.*, 1991, **58**, (16), pp. 1730–1732

6 MOHLMANN, G.R.: 'Polymeric optochips: splitters, switches and modulators', *Synth. Met.*, 1994, **67**, pp. 77–80

7 LEE, M.H., LEE, H.J., HAN, S.G., KIM, H.Y., WON, Y.H., and KANG, S.Y.: 'Fabrication and characterization of an electro-optic polymer waveguide modulator for photonic applications', *Thin Solid Films*, 1997, **303**, pp. 287–291

8 KIM SEONGKU, ZHANG, H., ZHANG, C., WANG, C., STEIER, W.H., and FETTERMAN, H.R.: 'Electro-optic polymer modulators with an inverted rib waveguide structure', *IEEE Photonics Technol. Lett.*, 2003, **15**, (2), pp. 218–220

9 ZHANG, C., DALTON, L.R., OH, M.C., ZHANG, H., and STEIER, W.H.: 'Low V_π electrooptic modulators from CLD-1: chromophore design and synthesis, material processing, and characterization', *Chem. Mater.*, 2001, **13**, pp. 3043–3050

10 KIM SEONGKU, GEARY, K., CHANG, D.H., FETTERMAN, H.R., ZHANG, H., ZHANG, C., WANG, C., and STEIER, W.H.: 'TM-pass polymer modulators with poling-induced waveguides and self-aligned electrodes', *Electron. Lett.*, 2003, **39**, (9), pp. 721–722

11 ZHANG, H., OH, M.-C., SZEP, A., STEIER, W.H., ZHANG, C., DALTON, L.R., CHANG, D.H., and FETTREMAN, H.R.: 'Push-pull electro-optic polymer modulators with low half-wave voltage and low loss at both 310 and 1550 nm', *Appl. Phys. Lett.*, 2001, **78**, (20), pp. 3136–3138

12 Data sheet from JDS UNIPHASE: '10 Gb/s dual drive modulator', product-code 210094480.

13 Data sheet from AGERE SYSTEMS: '40 Gbits/s lithium niobate electro-optic modulator', Rev. 2, DS99-365LWP-2, June 2001.

14 Data sheet from LUCENT TECHNOLOGIES: 'Using the lithium niobate modulator: electro-optical and mechanical connections', Technical Note, TN98-004LWP, April 1998.

15 VYDRA, J., BEISINGOFF, H., TSCHUDI, T., and EICH, M.: 'Photodecay mechanisms in side chain nonlinear optical polymethacrylates', *Appl. Phys. Lett.*, 1996, **69**, (8), pp. 1035–1038

16 TENG, C.C., MORTAZAVI, M.A., and BOUDOUGHIAN, G.K.: 'Origin of the poling-induced optical loss in a nonlinear optical polymeric waveguide', *Appl. Phys. Lett.*, 1995, **66**, (6), pp. 667–669